Enantiomer selectivity and energy transfer in imperfect chiral cavities

David Dams *
Karlsruhe Institute of Technology, Institute of Theoretical Solid State Physics, Kaiserstr. 12, 76131 Karlsruhe, Germany

Carsten Rockstuhl
Karlsruhe Institute of Technology, Institute of Theoretical Solid State Physics, Kaiserstr. 12, 76131 Karlsruhe, Germany and Karlsruhe Institute of Technology, Institute of Nanotechnology, Kaiserstr. 12, 76131 Karlsruhe, Germany

(Received 16 June 2025; accepted 27 August 2025; published 10 September 2025)

Chiral polaritonics offers promising opportunities to selectively manipulate molecular species based on their handedness by harnessing unique interaction pathways offered by strong coupling in cavity QED. While significant progress has been made in understanding the fundamental mechanisms of enantiomer selectivity, many existing studies focus on perfectly chiral cavities that contain only one type of enantiomer. Here, we investigate a scenario of imperfect cavities containing varying mixtures of enantiomers. Using a generalized Hopfield-type model, we systematically explore how the degree of enantiomeric mixing and cavity imperfections affect chiral selectivity. Our analysis includes both an examination of the cavity's eigenmode structure and a quantitative assessment of differential energy transfer into specific enantiomeric species. We demonstrate that both cavity imperfections and the presence of enantiomer mixtures profoundly modify the polaritonic dispersion. We also highlight that pushing the system into the deep strong coupling regime—by increasing molecular concentration—can decrease the efficiency of energy transfer to matter modes. These findings emphasize that precise cavity design and detailed consideration of enantiomeric composition are essential for achieving optimal chiral selectivity in practical cavity QED systems.

DOI: 10.1103/p4dp-byb8

I. INTRODUCTION

Chirality refers to the fundamental geometrical property of an object that cannot be superimposed onto its mirror image by a sequence of rotations and translations [1]. Many naturally occurring molecules exhibit chirality, rendering this property critically important across numerous aspects of human life, including biology [2], chemistry [3], pharmaceuticals [4], and technological applications [5]. Recently, substantial progress has been achieved in both theoretical modeling [6–16] and practical fabrication [17,18] of chiral optical cavities that selectively support photonic modes of distinct helicities. Progress has also been made in fabricating and optimizing individual emitters, such as certain quantum dots, to exhibit intrinsic properties or external control—such as maximized directionality-dependent coupling [19] or reduced decoherence [20]. This development has given rise to the emerging field of chiral polaritonics, where the combination of strong light-matter interactions (cavity QED) and intrinsic chiral selectivity enables novel possibilities, such as enantioselective detection [11,21], energy transfer [22,23], and enhancement of chemical reactions [24–26]—a prospect with significant implications for pharmaceutical synthesis and material science. Further promising theoretical results indicate the possibility of collective radiant behavior [27] and chirality-dependent photon transport [28].

Despite rapid advancements, several important theoretical and practical considerations remain underexplored. Notably, a hallmark of chiral polaritonics is the ability to achieve discriminatory ground-state energy splittings. The practical consequences of this discriminatory effect include enantiospecific differences in reactivity [6] as well as rotational spectra [7]. These splittings can be shown to scale as $\sqrt{N}$ for a cavity containing N molecules, extending deep into the ultrastrong coupling regime [6]. However, potential limitations arising from diminishing effective light-matter coupling, as anticipated due to diamagnetic contributions in the deep strong regime [29,30], have yet to be thoroughly investigated.

Moreover, the influence of cavity imperfections—arising from deviations in cavity geometry or symmetry—remains insufficiently understood, and theoretical analyses often rely on the simplifying assumption that the cavity contains only a single enantiomeric species. To address these limitations, our study incorporates both phenomenological parameters capturing cavity imperfections and the presence of enantiomers of opposite handedness.

In this work, we aim to address these gaps by connecting and building on previously established insights to achieve a deeper understanding of chiral cavity QED. Specifically, we employ a generalized Hopfield-type model to systematically

*Contact author: david.dams@kit.edu

explore the polaritonic eigenmode structure and energy transfer efficiency under conditions of varying coupling strengths (ranging from weak to deep strong), cavity imperfections, and enantiomeric mixtures.

This paper is structured as follows. In Sec. II, we introduce our theoretical framework, presenting a variant of the chiral Hopfield model and highlighting the critical role of the diamagnetic terms. Subsequently, in Sec. III, we investigate the polaritonic dispersion within a closed cavity. Our investigation is guided by a focus on the matter content contained in the polaritonic modes, which provides an intuitive way to understand how ultrastrong coupling, cavity imperfections, and enantiomeric mixtures influence the polaritonic characteristics. To complement and validate this analysis, Sec. IV focuses on evaluating the energy transfer efficiency when the cavity interacts with an external field. To this end, we use analytical expressions obtained from an S-matrix approach that is conceptually similar to previously established input-output theories [31–33]. Finally, in Sec. V, we summarize our findings and discuss their broader implications for the design of efficient and selective chiral polaritonic systems. As our analysis still focuses on lossless cavities, we include a brief comment on expected qualitative changes and identify key directions for future work when dissipation and losses are taken into account.

II. MODEL HAMILTONIAN

We consider a cavity supporting two helical photonic modes. The cavity contains enantiomers of different handedness. The coupled system can be described by the Hamiltonian

$$H = H_0 + H_{\text{light-matter}} + H_{\text{light-light}}. \tag{1}$$

The first term refers to an uncoupled oscillator ensemble composed of cavity modes, annihilated by $a_\pm$, and bosonic matter excitations, annihilated by $b_\pm$, given by [32]

$$H_0 = \sum_{i\in\{+,-\}} \omega_i^0 a_i^\dagger a_i + \omega_b \sum_{i\in\{+,-\}} b_i^\dagger b_i. \tag{2}$$

We have assumed the degenerate eigenfrequency ω_b for the chiral matter excitations and denoted the cavity mode eigenfrequencies as ω_i^0. As discussed in Ref. [6], the approximation of matter excitations as bosonic quasiparticles is justified in the low-excitation, collective limit. The interaction between photonic and matter components of the system can be expressed as [29]

$$H_{\text{light-matter}} = \sum_{m,n\in\{+,-\}} l_{mn}(a_m^\dagger + a_m)(b_n^\dagger + b_n), \tag{3}$$

where the light-matter coupling constants are modeled similar to Refs. [6,34] as

$$l_{mn} = \gamma_n(1 + g\cdot m\cdot n), \tag{4}$$

with the implicit identification $+\equiv 1, -\equiv -1$. The factor $\gamma_n \sim \sqrt{N_n}$ expresses the overall strength of the interaction, scaling with the square root of the number of enantiomers belonging to the nth species [6]. In the closely related model discussed in Ref. [34], it is given by

$$\gamma_n = \sqrt{\frac{\omega}{2\epsilon_0 V}}, \tag{5}$$

where V is the cavity volume, ϵ_0 the vacuum permittivity, and ω the wavelength of the chiral light. The chirality factor g relates the electric and magnetic transition dipole moments, $\vec{d}$ and $\vec{m}$, as follows:

$$g = \frac{\text{Im}[\vec{d}\vec{m}]}{|\vec{d}|^2}. \tag{6}$$

The type of coupling is determined by the ratio $\frac{\gamma_n}{\omega_b}$ [29]. For $\gamma_n < 0.1\omega_b$, the rotating wave approximation (RWA), obtained by neglecting the counterrotating terms in Eq. (1), holds well and the system can be described by a Hamiltonian similar to the Jaynes-Cummings model [35]. Taking into account the magnitude of the dissipation rates of light and matter subsystems allows for the further subdivision of this region into weak and strong coupling regimes [35]. Since the present investigation is not focused on dissipative processes, we refer to this regime broadly as the RWA-applicable region. The ultrastrong coupling limit (USC), where $\gamma_n \gtrapprox 0.1\omega_b$, implies the breakdown of the RWA, while a perturbation theory clearly separating the light and matter degrees of freedom becomes inapplicable already in the strong coupling limit. Finally, increasing the coupling even further, so that $\gamma_n \approx \omega_b$ and beyond, defines the deep strong coupling regime (DSC). In this regime, any perturbative treatment becomes ineffective, and the system is only described correctly by joint light-matter excitations, termed polaritons.

The chirality of matter in this description is captured by the parameter g and ultimately originates from magnetic dipole interactions [34,36]. While ideally chiral matter completely decouples from the cavity mode of opposite handedness and is thus characterized by $g = \pm 1$, values for typical molecular systems are much smaller in magnitude [6]. For the majority of our investigations, we focus on a concrete illustrative value of $g = 0.01$ and only depart from it in our discussion of Fig. 3. Lastly, the diamagnetic (self-)interaction of cavity photon modes is given by

$$H_{\text{light-light}} = \sum_{i,j\in\{+,-\}} D_{ij}(a_i^\dagger + a_i)(a_j^\dagger + a_j). \tag{7}$$

The coupling constants D_{ij} can be inferred from the requirement of vanishing ground-state currents by the Thomas-Reiche-Kuhn (TRK) sum rule [37,38]. Analogous to Refs. [29,30,32], we determine them to be

$$\sum_{n,m\in\{+,-\}} \frac{l_{ni}\bar{l}_{mj}}{\omega_b} = D_{ij}. \tag{8}$$

Neglecting the diamagnetic terms is typically a safe assumption for the weak coupling limit [29]. However, as pointed out in Refs. [29,38,39], beyond this regime, discarding diamagnetic effects leads to incorrect model behavior. In the DSC regime, the diamagnetic term drastically reduces the light-matter interaction strength, effectively decoupling the cavity modes and matter [29]. For these reasons, we explicitly retain the diamagnetic term in our model.

Similarly, the commonly employed rotating wave approximation, obtained by neglecting antiresonant terms coupling two creators or annihilators, can not be expected to provide reliable results in the USC regime [40,41]. For that reason, our model includes both resonant and antiresonant terms.

The Hamiltonian in Eq. (1) can be diagonalized by the usual Hopfield-Bogoliubov procedure [37] to obtain

$$H = \sum_i \omega_i \beta_i^\dagger \beta_i. \tag{9}$$

The polaritonic operators β_i, as entries of a vector β, are associated with eigenfrequencies ω_i. Collecting photonic and matter modes in the vector

$$c \equiv \begin{pmatrix} a_1 \\ a_{-1} \\ b_1 \\ b_{-1} \end{pmatrix}, \tag{10}$$

the vector of polaritonic operators β is obtained via the linear transformation T

$$\beta = \begin{pmatrix} p \\ p^\dagger \end{pmatrix} = T \begin{pmatrix} c \\ c^\dagger \end{pmatrix}, \tag{11}$$

where p, c, $p^\dagger$, $c^\dagger$ denote column vectors. In the following, we distinguish the radiation and matter modes from the (noninteracting) polaritonic eigenmodes of the cavity by referring to the former as bare modes.

The model described by Eq. (1) is closely related to standard representations of chiral cavities [6,34] when one cavity mode is neglected. In Appendix A, we demonstrate that the correlated ground state energy derived from our Hamiltonian exhibits the expected scaling behavior with the square root of the enantiomer number, consistent with *ab initio* calculations [7]. We take this as an indication that our model is capable of qualitatively predicting physical phenomena in realistic systems.

In the following, we study the impact of mode imperfections and enantiomeric mixtures on the ability of the cavity to discriminate efficiently between matter of differing chirality. We will focus on the properties of a closed cavity first. For that, we study the resulting modifications to the polariton dispersion in Sec. III, using an intuitive measure of chiral selectivity in terms of the difference in positive and negative chirality matter content directly derived from the polaritonic eigenvectors. Having gained a conceptual understanding of the closed cavity, we compute the differential energy transfer efficiency from an external source employing an S-matrix approach to supplement and validate these findings in Sec. IV. We expect this differential energy transfer to be a potential key quantity, e.g., for enantioselective catalysis, and point out its relation to the intuitive selectivity measure.

To limit the main investigation to the essential physics at play, we preemptively constrain the parametric freedom in our model by considering the positive and negative helicity modes of the photonic sector to occupy degenerate eigenfrequencies. The case of spectrally detuned cavity modes is considered separately in Appendix B.

III. POLARITON DISPERSION

A. Perfectly chiral cavity, single-handed matter

The primary purpose of chiral cavities is their ability to selectively address different enantiomers. An often considered scenario focuses on a chiral cavity supporting a single mode of pure helicity containing a single enantiomer species [6]. In this section, we first revisit this scenario and study the properties of the associated polaritonic modes. We then contrast this with the behavior of the system when the assumptions of enantiomeric purity and cavity perfection are forgone.

Aside from their eigenfrequencies, a useful property characterizing cavity polaritons is their similarity to the bare modes. For the ith polaritonic mode, the contribution it receives from the jth bare mode is defined as [29]

$$C_j^i = \frac{|T_{ij}|^2}{\sum_k |T_{ik}|^2}, \tag{12}$$

where the matrix entries T_{ij} compose the linear transformation in Eq. (11). As noted in Ref. [29], this quantity converges to 1 for a polariton consisting purely of the jth bare mode. Such a behavior assigns it the role of an indicator of (de)coupling, since a polariton mixing different bare modes is generically expected to facilitate enhanced interaction between them. While its primary purpose is to illustrate the fundamental physical processes involved in the chiral polariton model studied here, its qualitative connection to experimental observables is discussed in Ref. [29]. For instance, the spontaneous emission rate attains its maximum if C_j^i indicates a perfect mixture of light and matter [29]. This argument is solidified in Appendix C, where a close connection between Eq. (12) and the energy transfer efficiency from an external source is demonstrated, forming the basis of Sec. IV. For simplicity, we denote the positive and negative matter content of the ith eigenmode by C_+^i and C_-^i, respectively.

We first recapitulate the familiar case of a perfectly chiral cavity containing a single type of enantiomer by setting $\gamma_- = 0$ in Eq. (1) and disregarding the mode of negative helicity. As a result, the light-matter coupling matrix l_{nm} in Eq. (4) is reduced to a single, nonzero entry l_{++}. We consider the impact of the coupling parameter γ_+ on the polaritonic dispersion and the matter content of the associated modes. The results for an exemplary system are displayed in Fig. 1. Increasing the coupling strength leads to the usual level repulsion behavior of the upper and lower polaritonic branches in the strong coupling limit [42]. For small values of the coupling constant γ_+, the matter content of the polaritonic modes allows them to be well identified with those of an uncoupled system. For our exemplary system, the lower polariton remains a matter-dominated state, while the upper polariton predominantly comprises light. Increasing γ_+ leads to a larger degree of light-matter mixture, as the two bare modes undergo stronger coupling. Notably, and in agreement with previous results [29], this is not a monotonous trend, as the diamagnetic terms in Eq. (7) reduce the effective coupling strength. Into the DSC regime, where $\gamma_+ > 1$, the effective coupling diminishes: the matter content of the lower polariton becomes dominant again, while the upper polariton reverts to a mostly photonic state. While these results are consistent with established behavior in nonchiral systems, their implications

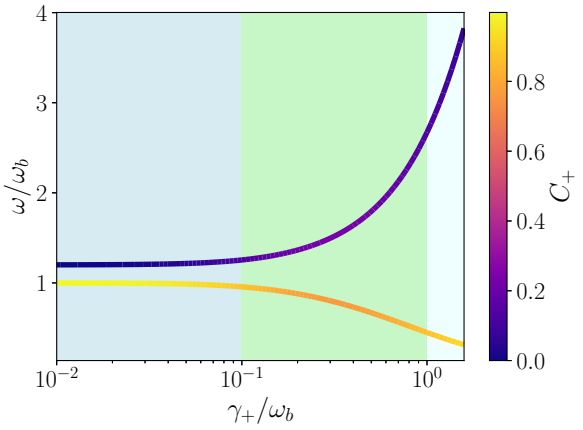

FIG. 1. Polaritonic eigenfrequencies ω, normalized by the matter excitation frequency ω_b annotated by matter content C_+. Different coupling regimes, as defined in the main text, are indicated by background colors: the RWA-applicable region is indicated by a blue background, while the DSC and USC regimes are marked by green and cyan hues, respectively. The cavity contains a single type of enantiomer with $g = 0.01$ and supports only one mode of positive helicity at $\omega_+^0 = 1.2\omega_b$. The lower polariton is matter dominated at low coupling strength, whereas the upper polariton is primarily photonic. As the interaction strength γ_+ grows, light and matter are more mixed. However, this behavior is nonmonotonous. When approaching the DSC regime, *i.e.*, where $\gamma_+/\omega_b > 1$, the effective coupling decreases, leading the lower polariton to regain matter dominance, while the upper polariton increasingly loses its matter content.

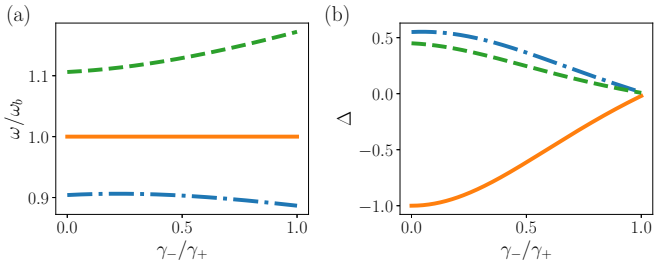

FIG. 2. (a) Polaritonic eigenfrequencies ω. The cavity is considered at resonance with $\omega_+^0 = \omega_b$. Enantiomers of both chiralities are present with $g = 0.01$ and γ_+ is set to $0.1\omega_b$. The branches originating at $\omega \sim 0.9\omega_b$ and $\omega \sim 1.1\omega_b$ (dashed and dotted line) correspond to the lower and upper polaritonic branches visible in Fig. 1, while a third branch at ω_b (solid line) emerges. (b) Excess content of positive chirality matter, Δ, defined in the main text, where identical line styles encode identical polaritons to those in (a). Increasing γ_-, positive and negative matter components mix in all modes, slightly increasing the splitting between upper and lower polariton branches. The excess content of positive chirality matter in the upper and lower polaritons diminishes, signifying suppressed chiral selectivity.

in the context of chiral light-matter coupling have not yet been explored.

B. Perfectly chiral cavity, mixed-handed matter

We now turn to the additional presence of enantiomers of the opposite handedness. The key property of interest is the discriminatory interaction of the cavity with different enantiomeric species. To this end, we operationalize this chiral selectivity as the difference in matter content of positive and negative handedness, defined as

$$\Delta^i = C_+^i - C_-^i. \tag{13}$$

As equal mixing of positive and negative chiral matter modes with light is not expected to facilitate chirality-sensitive interactions, larger values of Δ indicate an increase in chiral selectivity.

We start by considering nonzero values for γ_-, while keeping the negative helicity cavity mode turned off. Consequently, the light-matter coupling matrix l_{nm} in Eq. (4) contains two nonzero entries, l_{++} and l_{+-}. The results are displayed in Fig. 2 for a resonant system at $\gamma_+/\omega_b = 0.1$. The introduction of enantiomers of negative handedness leads to the appearance of a third polaritonic branch. In the limit $\gamma_- = 0$, this branch can be identified with a noninteracting matter mode of pure negative chirality (solid line in Fig. 2), while the two branches energetically surrounding it correspond to the upper and lower polaritons in Fig. 1 (dashed and dotted line in Fig. 2). Upon increasing γ_-, negative and positive matter components mix, as manifested by a decreasing value for Δ in the upper and lower polariton branches. The magnitude of Δ decreases also for the branch at ω_b, and it tends from a larger negative value to zero. Upon racemization at $\gamma_+ = \gamma_-$, the excess matter content of positive chirality in the lower and upper polaritons is greatly reduced, indicating suppressed selectivity even in a perfectly chiral cavity. This finding of suppressed chiral selectivity under racemic conditions, even within a perfectly chiral photonic environment, has not been previously highlighted.

The results above have been obtained for relatively weakly chiral matter, expected for most naturally occurring molecules [43]. Thus, one might anticipate that matter possessing a stronger intrinsic chirality could better preserve the selective advantages offered by a perfectly chiral cavity. This expectation indeed holds true. To illustrate this, we specifically examine the adiabatic continuations of the upper and lower polariton branches. As clearly shown in Fig. 3, the excess content of positive chirality matter remains consistently elevated when the intrinsic chirality parameter, g, takes higher values (typically above 0.5). In particular, the limit $g = 1$ corresponds to a scenario where negative chirality matter completely decouples from the cavity mode that is designed to couple to the positive chirality matter. Consequently, variations in the coupling parameter γ_- cease to influence the system dynamics in this regime. This underscores that strong intrinsic chirality effectively shields the polaritonic modes from undesirable mixing, thereby robustly maintaining the cavity's chiral selectivity.

C. Imperfect cavity, mixed-handed matter

We now investigate the effect of cavity imperfections, manifesting themselves through the introduction of cavity modes with opposite helicity, thereby diminishing the cavity's ability to interact with enantiomers selectively. In this scenario,

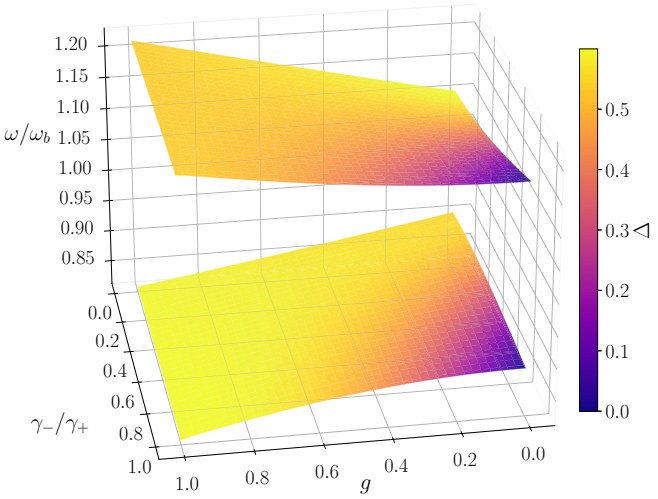

FIG. 3. Polaritonic eigenfrequencies, annotated by Δ, as a function of γ_-/γ_+ and intrinsic matter chirality g. All remaining parameters are identical to Fig. 2. The plot highlights how a stronger intrinsic chirality ($g \gtrsim 0.5$) preserves the excess positive chirality matter content in the upper and lower polariton branches. In the perfect-chirality limit ($g = 1$), negative chirality matter fully decouples from the cavity mode, making the system dynamics insensitive to variations in γ_-. Such a decoupling demonstrates that strong intrinsic chirality effectively protects polaritonic modes from undesirable mixing and preserves the chiral selectivity initially provided by the cavity.

the light-matter coupling matrix l_{nm} in Eq. (4) is taken into account. To systematically study this effect, we follow an approach similar to that described in Ref. [34], by scaling the coupling strengths of the negative helicity mode through a dimensionless parameter d defined as

$$l_{-n} \to d \cdot (1 - g \cdot n). \tag{14}$$

In this way, the negative helicity mode can be gradually switched on from $d = 0$ and then tuned to a fully achiral cavity at $d = 1$. In Fig. 4, results are displayed for a resonant system filled with a racemic mixture at $\gamma_+/\omega_b = 0.1$. The four bare modes (two light and two matter excitations) lead to the emergence of four polaritonic modes. The energetically highest and lowest lying remain identifiable with the upper and lower polaritonic modes discussed so far. They undergo a further split while the additional two modes remain mostly inert energetically and localized around ω_b. While the system initially favors positive chirality, this advantage tends towards numerical zero at $d = 1$, where the cavity becomes achiral, as shown in Fig. 4(b).

Moreover, the reduction in positive matter content follows a highly nonlinear trend and occurs predominantly for relatively large values of the parameter d. This suggests a certain resilience of the system's chiral selectivity against moderate imperfections. Only when cavity imperfections become pronounced, approaching full achirality, does the system significantly lose its preferential coupling to positive chirality matter.

Lastly, we study the interplay of cavity imperfections and degree of enantiomeric mixture by investigating the

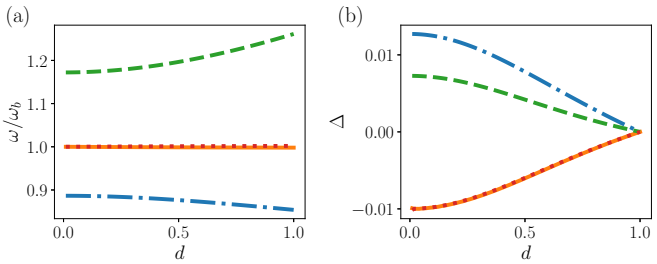

FIG. 4. (a) Polaritonic eigenfrequencies ω as a function of the phenomenological cavity imperfection parameter d. The negative and positive chirality photon modes are considered energetically degenerate with $\omega_+^0 = \omega_-^0$, and the cavity is filled with a racemic mixture with $\gamma_+ = \gamma_-$. All remaining parameters are identical to Fig. 2. Four polaritonic modes emerge from the bare two light and two matter excitations. The highest and lowest modes are identifiable as upper and lower polaritons, undergoing additional splitting, while the remaining two modes remain energetically stable and localized near ω_b. (b) Excess content of positive chirality matter, Δ, defined in the main text, where identical line styles encode identical polaritons to those in (a). The excess positive chirality content initially favors positive chirality matter but progressively diminishes toward zero as the cavity approaches full achirality ($d = 1$). The strongest reduction in chiral selectivity occurs primarily at large values of d.

characteristics of the adiabatically continued upper and lower polaritonic branches as a function of γ_- and d. The results displayed in Fig. 5 illustrate a largely complementary effect exhibited by both parameters: the energetic split is magnified and the chiral selectivity Δ is reduced. However, the dominant impact on the reduction of Δ can be ascribed to the presence of opposite-handedness enantiomers, encoded in γ_-, while the cavity imperfection d plays a much less pronounced role.

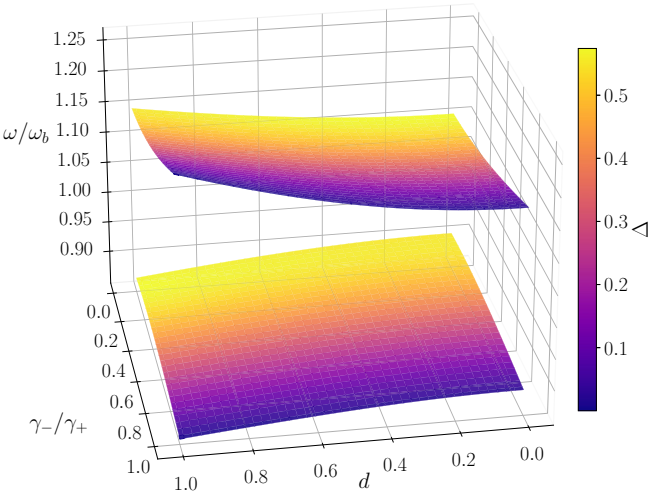

FIG. 5. Polaritonic eigenfrequencies ω, as a function of γ_-/γ_+ and cavity imperfection d. The system is characterized by otherwise identical parameters as those in Fig. 2. The adiabatically continued upper and lower polaritonic branches reveal the complementary roles of cavity imperfections (d) and enantiomeric mixture (γ_-). Increasing either parameter enhances the energetic splitting while simultaneously reducing the chiral selectivity Δ, highlighting their combined detrimental impact on chiral selectivity.

Although the influence of cavity imperfections has been previously considered, the present analysis reveals a previously underexplored robustness of chiral selectivity against moderate photonic imperfections. Notably, significant degradation of selectivity only arises near the fully achiral limit, underscoring the dominant role of molecular composition over cavity symmetry in determining chiral discrimination.

To summarize this section, we have first shown that increasing the coupling strength initially enhances matter-light interactions but eventually leads to a diminishing effective coupling in the USC regime. Second, introducing mixtures of enantiomers reduces chiral selectivity in a perfectly chiral cavity, though strongly chiral matter can counteract this loss by effectively decoupling the undesired enantiomer. Third, cavity imperfections that introduce modes of opposite helicity cause a nonlinear but significant decline in chiral selectivity, especially at high levels of imperfection. Fourth, enantiomeric mixtures and cavity imperfections act in tandem, collectively magnifying the loss of chiral discrimination and emphasizing the necessity of careful system design to maintain optimal selectivity.

IV. ENERGY TRANSFER EFFICIENCY

In the preceding section, we developed a physical understanding of how cavity imperfections and enantiomeric mixtures influence polariton characteristics, especially the chiral selectivity defined in Eq. (13). We now validate and supplement this analysis by considering the system under external illumination. In particular, we will study how the coupling coefficients of the photonic cavity modes to an external classical field and the degree of enantiomeric mixture influence the energy transfer efficiency.

For this purpose, we introduce a classical field $\phi(t)$ that excites the system at the initial time $t = 0$ with amplitude A_0, as follows:

$$\phi(t) = A_0\delta(t). \tag{15}$$

Its interaction with the cavity modes is given by the following Hamiltonian:

$$H_{\text{int}}(t) = \phi(t)(c_- a_- + c_+ a_+) + \text{H.c.}, \tag{16}$$

where we have introduced the coupling coefficients c_-, c_+ to parametrize the electromagnetic selectivity of the cavity. At $c_- = 0$, light of negative helicity is completely prevented from interacting with the cavity, similar to established proposals for realizing chiral cavities [10]. We choose these coefficients frequency-independent [32] and real [29]. Building on the insights from earlier established studies that employed input-output approaches to describe cavity behavior [31,44], these parameters closely correspond to those arising in a full quantum treatment of coupled modes inside and outside the cavity, as derived from the complete Maxwell solutions for a specific system. We determine the S matrix from Eq. (16) that maps incoming to outgoing states as

$$|\psi_{\text{out}}\rangle = S\,|\psi_{\text{in}}\rangle\,, \tag{17}$$

where the outgoing state is considered at temporal infinity. As the incoming state, we choose the joint polaritonic vacuum, defined by

$$p_i\,|0\rangle = 0, \tag{18}$$

for all operators p_i. The expected energy transfer to a matter mode is then given by

$$\Delta E_i = \omega_b\,\langle\psi_{\text{out}}|\left(b_i^I\right)^\dagger b_i^I|\psi_{\text{out}}\rangle\,, \tag{19}$$

where the operator b^I is taken in the interaction picture at temporal infinity. As shown in Appendix C, the energy transfer can be obtained analytically using standard manipulations. To this end, we write the inverse transformation of Eq. (11) as

$$T^{-1} = \begin{pmatrix} X & \overline{Y} \\ Y & \overline{X} \end{pmatrix}, \tag{20}$$

with submatrices X and Y. Following the derivation in Appendix C, the energy transfer can be determined from these matrices according to

$$\Delta E_i/\omega_i^0 = |z_i|^2 + \sum_i Y_{ij}\overline{Y}_{ij}. \tag{21}$$

The c number z_i is given by

$$z_i = \sum_j \overline{X}_{ij}\phi_j + \sum_j Y_{ij}\overline{\phi}_j, \tag{22}$$

where

$$\phi_j = -i\sum_l C_l(\overline{X}_{lj} + \overline{Y}_{lj}). \tag{23}$$

The quantities above have an intuitive interpretation: ϕ_j represents the sum of light-matter contributions to the jth polariton. These contributions are weighted by their associated coupling coefficients. In turn, z_i projects these weighted polaritonic sums back onto the ith bare mode. Finally, we define the energy transfer efficiency η_i to a given mode as the fraction of the total transferred energy it receives

$$\eta_i = \frac{\Delta E_i}{\sum_j \Delta E_j}. \tag{24}$$

From the discussion above, we observe a close similarity between the implications of the current expression and those of Eq. (12). The underlying physical reasoning behind using Eq. (12) is that polaritonic modes exhibiting purely photonic or purely matter characteristics do not facilitate enhanced light-matter interactions. This principle is captured explicitly in Eq. (24): since the coupling coefficients C_i isolate the components of the polariton that interact with external illumination (i.e., the cavity modes), the efficiency of energy transfer into matter modes diminishes when the polaritonic modes become purely photonic or purely matterlike.

It is instructive to contrast our approach with established methods based on input-output theory. In such frameworks, the system is partitioned into electronic and optical input and internal quantities, with the latter integrated out, leading to an effective non-Hermitian, dissipative dynamics governed by quantum Langevin equations [32]. By contrast, our method retains a fully Hermitian, closed-system description: we compute the exact S matrix for a unitary evolution under a time-dependent Hamiltonian, incorporating the external excitation via a classical field. This approach is closely related

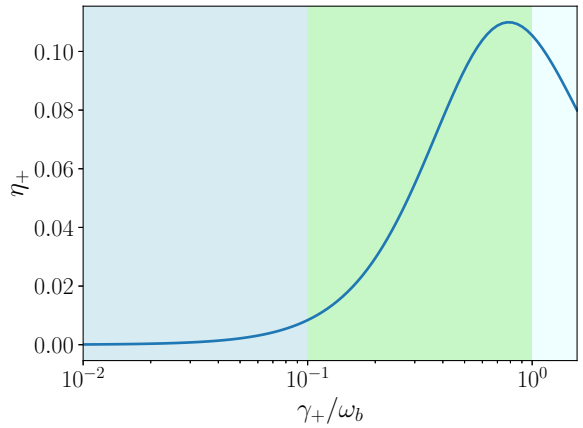

FIG. 6. Energy transfer efficiency η_+ for a cavity supporting a single positive helicity mode containing enantiomers of positive chirality only. The efficiency is not a monotonous function of γ_+, but rather declines considerably in the DSC regime. The external illumination is coupled to the cavity mode with $c_+ = 1$, while all other parameters are identical to those in Fig. 1. The coupling regimes of RWA-applicable, USC, and DSC regions are indicated by identical background colors as in Fig. 1.

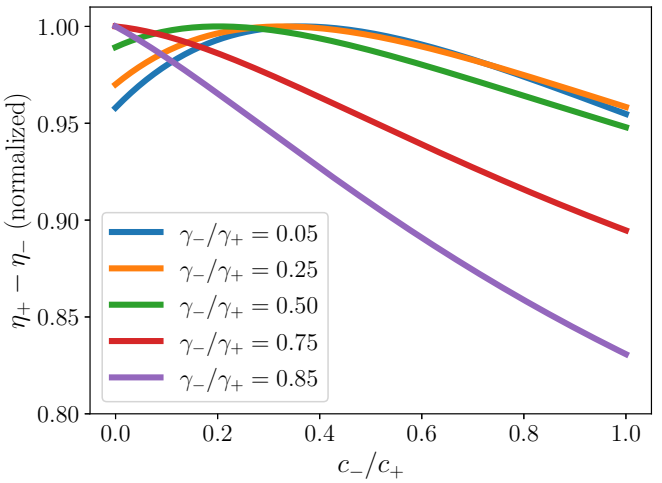

FIG. 7. Differential energy transfer efficiency $\eta_+ - \eta_-$, as a function of the external coupling ratio c_-/c_+ for different values of the ratio of enantiomeric coupling constants, γ_-/γ_+. The dependence on c_-/c_+ is not strictly monotonous for all degrees of enantiomeric mixtures. In particular, for smaller values of γ_-/γ_+, the differential efficiency initially increases with c_-/c_+ and reaches a variable peak before declining again. The appearance of the peak can be attributed to the fact that the presence of negative handedness enantiomers and negative helicity modes facilitates new interaction pathways for energy to be transferred to the positive handedness enantiomer, compared to a purely chiral cavity. This suggests that optimizing a cavity of this type for enantioselectivity may require the presence of opposite-handedness modes. In contrast, for larger γ_-/γ_+ values, the efficiency decreases monotonically with increasing c_-/c_+, reflecting a shift in the balance of enantiomeric interactions that suppresses this beneficial indirect coupling. We have checked numerically that a racemic mixture at $\gamma_- = \gamma_+$ exhibits a differential efficiency of zero at $c_- = c_+$, as expected.

to the paradigm of time-dependent perturbation theory, and the resulting redistribution of energy reflects enantioselective excitation differences in the final, mixed light-matter state. Notably, genuine dissipative effects, although neglected here, can still be incorporated on phenomenological grounds.

A. Transfer in a perfect cavity

We illustrate the immediate consequence of this correspondence in Fig. 6, where we display the energy transfer efficiency for a perfectly chiral cavity as a function of the coupling parameter γ_+. The corresponding closed cavity has been studied in Sec. III A. The energy transfer efficiency is notably enhanced as the system transitions into the strong and ultrastrong coupling regimes. However, as the coupling strength further increases into the DSC regime, characterized by $\gamma_+ > \omega_b$, the efficiency begins to decline. This behavior aligns well with previous findings [29] and is consistent with the discussions presented in Fig. 1. It is important to emphasize that while the efficiency of energy transfer to the matter modes decreases in this regime, the absolute amount of energy deposited continues to rise monotonically with increasing coupling strength γ_+. Consequently, even though stronger coupling facilitates greater total energy transfer, it simultaneously leads to a reduced efficiency. Practically, this indicates that increasing molecular concentration within the cavity can elevate the overall deposited energy (and thus potentially enhance processes such as reaction rates), but at the cost of a reduced efficiency. Aside from its novelty in its present form, this finding implies fundamental limits on the efficiency of enantioselective energy transfer at deep strong coupling in chiral polaritonics.

B. Transfer in an imperfect cavity

Based on these insights, we again focus on the USC regime where the highest possible coupling efficiency is achieved, and we consider a two-mode cavity filled with a resonant enantiomeric mixture to compute the differential energy transfer efficiency $\eta_+ - \eta_-$. Figure 7 displays the impact of opening the interaction channel to external light of negative helicity for different chiral coupling parameters γ_-/γ_+. Notably, the functional dependence of $\eta_+ - \eta_-$ does not present itself as strictly monotonous.

For smaller values of the coupling ratio γ_-/γ_+, the differential energy transfer efficiency exhibits a distinctly nonmonotonous dependence on the ratio c_-/c_+. Initially, as c_- increases from zero, we observe an enhancement in the differential efficiency, peaking at a finite, nonzero value of c_-. Following this peak, further increases in c_- result in a noticeable decline. This behavior can be understood by considering that the hybridization between cavity modes is inherently bidirectional: introducing an external excitation channel for the negative helicity mode (increasing c_-) does not merely siphon energy away from the positive helicity mode. Instead, it activates indirect interaction pathways concurrently, enabling additional energy flow into the positive helicity mode, thereby boosting the differential efficiency in an intermediate parameter range. Conversely, for larger values of γ_-/γ_+, the differential energy transfer efficiency monotonically decreases with increasing c_-. This basic behavior

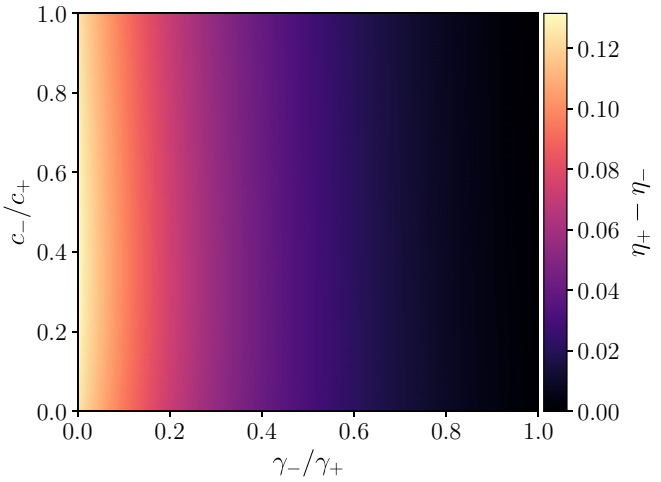

FIG. 8. Differential energy transfer efficiency $\eta_+ - \eta_-$ depending on external coupling c_-/c_+ and enantiomer coupling γ_-/γ_+. The trend observed in Fig. 7 is visible: form smaller values of the enantiomer coupling, $\eta_+ - \eta_-$ follows a nonmonotonous trend. The larger impact in reducing the absolute value of the differential efficiency is clearly played by the enantiomer coupling.

arises because the balance of enantiomeric interactions fundamentally shifts under these conditions, effectively reversing the previously beneficial indirect coupling pathways into predominantly detrimental ones close to racemization. A more complete picture is presented in Fig. 8.

Our analysis underscores the subtle interplay between cavity chirality, coupling symmetry, and external excitation conditions. Properly tuning these parameters is crucial for optimizing chiral selectivity and energy transfer efficiency, highlighting the necessity of carefully engineered cavity configurations to leverage USC regimes effectively.

V. CONCLUSION

In conclusion, our study has systematically explored the interplay between cavity chirality, intrinsic molecular handedness, and imperfections arising from cavity design and enantiomeric mixtures. Utilizing a generalized Hopfield-type model, we revealed that while enhancing the coupling strength initially improves chiral selectivity and energy transfer efficiency, deeper progression into the USC regime eventually diminishes the effective light-matter interaction due to diamagnetic effects. Furthermore, the presence of enantiomeric mixtures introduces additional complexity, notably reducing the differential chiral selectivity even in ideally chiral cavities. Importantly, our analysis has shown that strongly chiral matter can partially mitigate this reduction by effectively decoupling from undesired interaction channels.

Cavity imperfections, which manifest as unintended coupling to modes of opposite helicity, exacerbate this loss of selectivity. While moderate imperfections have limited effects, significant deviations from ideal cavity conditions rapidly degrade chiral discrimination. Importantly, we demonstrated that cavity imperfections and enantiomeric mixtures interact synergistically, significantly amplifying their detrimental impact on selectivity.

Although we have incorporated imperfections within a Hermitian framework and extended the model with that toward a form of pseudoloss, our analysis does not include the effects of realistic cavity dissipation. For moderate loss rates, we anticipate that energy transfer predictions derived from our S-matrix approach will qualitatively align with normalized integrated absorption spectra. However, genuine decoherence mechanisms, such as those arising from molecular vibrations, may significantly suppress effective light-matter coupling and limit enantioselective catalytic processes [45]. A promising direction for future work involves extending this framework via a full input-output theory or *ab initio* quantum electrodynamical treatments, to more accurately capture the role of dissipation and noise.

Ultimately, our findings highlight the necessity of carefully balancing molecular concentrations, intrinsic chirality, and cavity design imperfections to maintain optimal chiral selectivity and energy transfer efficiency. The nuanced understanding developed here provides valuable guidance for the future design and experimental realization of efficient and selective chiral polaritonic systems.

ACKNOWLEDGMENT

D.D. and C.R. acknowledge support by the German Research Foundation under Grant No. RO 3640/14-1 within Project No. 465163297.

DATA AVAILABILITY

The data that support the findings of this article are openly available [46].

APPENDIX A: GROUND-STATE ENERGY SCALING

Denoting the ground-state energy of a perfectly chiral cavity supporting only a single positive helicity mode filled only with enantiomers of positive (negative) chirality by E_+ (E_-), we define

$$\delta E = E_+ - E_-. \tag{A1}$$

As discussed in Refs. [6,7], this quantity follows a square-root behavior as a function of the number of enantiomers N, which in turn scales with $\sqrt{N} \sim \gamma_\pm$. In Fig. 9, we demonstrate this behavior as additional validation of our model in Eq. (1).

APPENDIX B: CAVITY MODE DETUNING

In the main text, we have always considered spectrally degenerate cavity modes with $\omega_+^0 = \omega_-^0$. To model more realistic proposals for chiral cavities [10], we forgo this assumption and introduce a spectral detuning between the two modes as follows:

$$\Delta\omega = \omega_-^0 - \omega_+^0. \tag{B1}$$

Figure 10 displays the differential energy transfer computed according to Eq. (24). Similar to the effect of negative-enantiomer coupling displayed in Fig. 10, we observe a nonmonotonous trend.

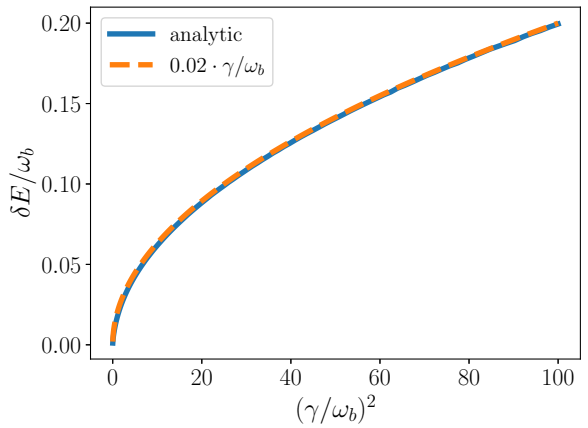

FIG. 9. Difference in correlated ground-state energies of a resonant cavity with a single mode of perfect positive helicity, where $\gamma_+ = \gamma_- = \gamma$. The number N of molecules is proportional to $(\gamma/\omega_b)^2$. Enantiomeric chirality is determined by $g = 0.01$. The dashed orange line following $\delta E = 0.02\gamma/\omega_b \sim 0.02\sqrt{N}$ serves as a guide to the eye.

APPENDIX C: *S*-MATRIX APPROACH

In the following, we derive the S matrix for a matter-loaded cavity coupled to a classical external field in natural units. Our analysis is conceptually similar to the cavity input-output formalism presented, e.g., in Refs. [30,31], but replaces the quantum Langevin equation with a unitary S matrix. Our model describes a collection of N bare bosons annihilated by operators c_i, $i \in [1, N]$, coupled to a classical external source, described by the N-vector f, assumed to be of compact temporal support. The general Hamiltonian is then given by

$$H = \begin{pmatrix} c^\dagger & c \end{pmatrix} \begin{pmatrix} A & B \\ \overline{B} & \overline{A} \end{pmatrix} \begin{pmatrix} c \\ c^\dagger \end{pmatrix} + \begin{pmatrix} f & \overline{f} \end{pmatrix} \begin{pmatrix} c \\ c^\dagger \end{pmatrix} \tag{C1}$$

$$\equiv \alpha^\dagger D \alpha + \begin{pmatrix} f & \overline{f} \end{pmatrix} \begin{pmatrix} c \\ c^\dagger \end{pmatrix}, \tag{C2}$$

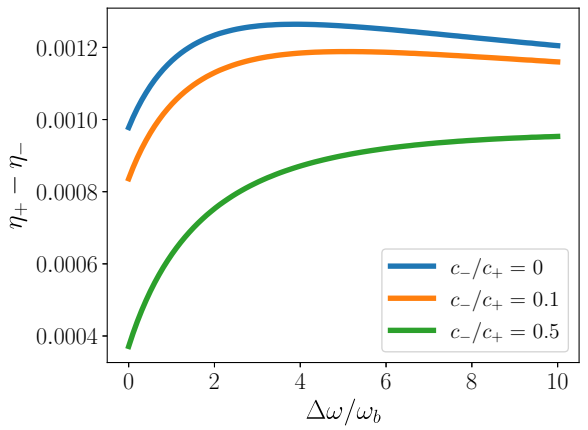

FIG. 10. Differential coupling efficiency $\eta_+ - \eta_-$ for different values of the coupling ratio c_-/c_+. The considered cavity contains a racemic mixture and all other parameters are identical to the ones used in Fig. 7.

where couplings have been absorbed into the classical fields and the matrix D denotes the kernel of the Hamiltonian. Notably, setting $f = 0$, our model introduced in Eq. (1) is of this form. The kernel can be diagonalized by a transformation effected by the matrix T. This leads to the basis of polaritonic operators β_i, introduced in Eq. (11), describing an uncoupled bosonic system with eigenfrequencies ω_i. Denoting by 1_N the identity matrix in N dimensions, we define

$$G = \begin{pmatrix} 1_N & 0 \\ 0 & -1_N \end{pmatrix}. \tag{C3}$$

The diagonalizing transformation T and its inverse can be expressed in terms of submatrices X and Y [47] as follows:

$$T = \begin{pmatrix} X^\dagger & -Y^\dagger \\ -Y^T & X^T \end{pmatrix} \tag{C4}$$

$$T^{-1} = \begin{pmatrix} X & \overline{Y} \\ Y & \overline{X} \end{pmatrix}, \tag{C5}$$

where the submatrices are obtained from the eigenvectors of GD [47]. Inverting Eq. (11), the Hamiltonian takes the usual form for an ensemble of driven harmonic oscillators

$$H = \underbrace{\sum_i 2\omega_i p_i^\dagger p_i}_{H_0} \underbrace{- i \sum_i (F_i p_i - \overline{F}_i p_i^\dagger)}_{H_{\rm int}}, \tag{C6}$$

where we have neglected an additive constant and introduced the c vector of the transformed field as

$$F \equiv i(fX + \overline{f}Y). \tag{C7}$$

Going to the interaction picture via the transformation

$$U(t, t_0) = e^{-iH_0(t-t_0)}, \tag{C8}$$

we obtain

$$p_i^I = U^\dagger(t, t_0) p_i U(t, t_0) = p_i e^{-i2\omega_i t} \tag{C9}$$

$$|n_i\rangle^I = |n_i\rangle \tag{C10}$$

$$H_{\rm int}^I(t) = -i \sum_i F_i e^{-i2\omega_i t} p_i + i \sum_i \overline{F}_i e^{i2\omega_i t} p_i^\dagger, \tag{C11}$$

where n_i denotes the ith polariton number. The S matrix is the usual map of input and output states, set at $t = -\infty$ and $t = \infty$, respectively

$$|\Psi_{\rm out}\rangle \equiv S\,|\Psi_{\rm in}\rangle\,. \tag{C12}$$

The S matrix can be expressed as the time-ordered product

$$S = \mathcal{T} \exp\left[-i \int_{-\infty}^{\infty} {\rm d}t H_{\rm int}(t)\right], \tag{C13}$$

where $\mathcal{T}$ expresses time ordering. Alternatively, S can be computed via its Magnus expansion [48]

$$S = \exp\left[\Omega(\infty, -\infty)\right] \tag{C14}$$

$$\Omega(t, t') = \sum_{i=1}^{\infty} \Omega_i(t, t') \tag{C15}$$

$$\Omega_1(t,t') = -i\int_{t'}^{t} \mathrm{d}\tau H_{\mathrm{int}}(\tau) \tag{C16}$$

$$\Omega_2(t,t') = -\int_{t'}^{t}\mathrm{d}s\int_{t'}^{s}\mathrm{d}\tau[H_{\mathrm{int}}(s),H_{\mathrm{int}}(\tau)]. \tag{C17}$$

In our case, the Magnus expansion closes after the second term, resulting in

$$S = \exp\left[\int_{-\infty}^{\infty}\mathrm{d}t\sum_i -F_i e^{-i2\omega_i t}p_i + \overline{F}_i e^{i2\omega_i t}p_i^\dagger\right], \tag{C18}$$

where we have suppressed a phase without influence on expectation values. By defining

$$\phi_i \equiv \int_{-\infty}^{\infty}\mathrm{d}t\overline{F}_i(t)e^{-i2\omega_i t}, \tag{C19}$$

we note that S turns into a product of displacement operators creating coherent states labeled by ϕ_i

$$S = \prod_i D(\phi_i) \tag{C20}$$

$$D(\phi_i) = \exp(\phi_i p_i^\dagger - \overline{\phi_i}p_i) \tag{C21}$$

$$D(\phi_i)\left|0\right\rangle = \left|\phi_i\right\rangle. \tag{C22}$$

This agrees with standard results for driven bosonic modes [49], specialized to the multimode hybrid light-matter excitations at hand. Choosing the joint vacuum as the initial state, we obtain

$$\left|\Psi_{\mathrm{out}}\right\rangle = \prod_i D(\phi_i)\left|0\right\rangle = \prod_i \left|\phi_i\right\rangle. \tag{C23}$$

We can compute the energy transferred to the ith bare bosonic mode of bare frequency ω_i^0 as

$$\Delta E_i = \omega_i^0\left\langle\Psi_{\mathrm{out}}\right|\left(c_i^I\right)^\dagger(t)c_i^I(t)\left|\Psi_{\mathrm{out}}\right\rangle, \tag{C24}$$

at $t=\infty$. Using Eq. (11) and removing indeterminate phase factors via the standard causal prescription $\omega_i \to \omega_i + i0^+$, we obtain

$$\Delta E_i/\omega_i^0 = |z_i|^2 + \sum_i Y_{ij}\overline{Y}_{ij} \tag{C25}$$

$$z_i = \sum_j \overline{X}_{ij}\phi_j + \sum_j Y_{ij}\overline{\phi}_j. \tag{C26}$$

For the driving field, we consider a delta-peaked classical source. Coupling to the lth cavity channel is encoded by parameters C_l, $l\in[1,N]$. We model these coupling parameters as spectrally constant [32] and real [29], leading to

$$\phi_i = -i\sum_l C_l(\overline{X}_{li} + \overline{Y}_{li}), \tag{C27}$$

which are the expressions used in the main text. We now remark on the limitations and applicability of the assumption of a delta-peaked source. One may alternatively consider a Gaussian source, assumed to be normalized (the normalization prefactor cancels out when computing transfer efficiency) and centered at $t=0$ for simplicity, such that

$$f(t) = \frac{1}{\sqrt{2\pi\sigma^2}}e^{-\frac{t^2}{2\sigma^2}}. \tag{C28}$$

This modifies Eq. (C19) to

$$\phi_i = e^{-8\sigma^2\pi^2\omega_i^2}. \tag{C29}$$

Introducing the characteristic timescale T_i of the ith polariton oscillation as

$$T_i = \frac{2\pi}{\omega_i}, \tag{C30}$$

we infer that the delta-pulse approximation remains valid as long as the temporal width σ of the pulse is sufficiently small compared to this timescale, i.e.,

$$T_i \gg \sigma. \tag{C31}$$

We have verified numerically that our results remain qualitatively unchanged for values of σ up to approximately 10% of the smallest polaritonic timescale T_i.

[1] L. D. Barron, *Molecular Light Scattering and Optical Activity*, 2nd ed. (Cambridge University Press, Cambridge, 2004).

[2] J. Gal, Molecular chirality in chemistry and biology: Historical milestones, Helv. Chim. Acta **96**, 1617 (2013).

[3] M. Quack, Structure and dynamics of chiral molecules, Angew. Chem. Int. Ed. Engl. **28**, 571 (1989).

[4] E. Sanganyado, Z. Lu, Q. Fu, D. Schlenk, and J. Gan, Chiral pharmaceuticals: A review on their environmental occurrence and fate processes, Water Res. **124**, 527 (2017).

[5] J. Brandt, F. Salerno, and M. Fuchter, The added value of small-molecule chirality in technological applications, Nat. Rev. Chem. **1**, 0045 (2017).

[6] C. Schäfer and D. G. Baranov, Chiral polaritonics: Analytical solutions, intuition, and use, J. Phys. Chem. Lett. **14**, 3777 (2023).

[7] R. R. Riso, L. Grazioli, E. Ronca, T. Giovannini, and H. Koch, Strong coupling in chiral cavities: Nonperturbative framework for enantiomer discrimination, Phys. Rev. X **13**, 031002 (2023).

[8] C. Schäfer, M. Ruggenthaler, and A. Rubio, *Ab initio* nonrelativistic quantum electrodynamics: Bridging quantum chemistry and quantum optics from weak to strong coupling, Phys. Rev. A **98**, 043801 (2018).

[9] H. Hübener, U. D. Giovannini, C. Schäfer, J. Andberger, M. Ruggenthaler, J. Faist, and A. Rubio, Engineering quantum materials with chiral optical cavities, Nat. Mater. **20**, 438 (2021).

[10] K. Voronin, A. S. Taradin, M. V. Gorkunov, and D. G. Baranov, Single-handedness chiral optical cavities, ACS Photon. **9**, 2652 (2022).

[11] Y.-H. Kang, Z.-C. Shi, J. Song, and Y. Xia, Effective discrimination of chiral molecules in a cavity, Opt. Lett. **45**, 4952 (2020).
[12] N. S. Baßler, A. Aiello, K. P. Schmidt, C. Genes, and M. Reitz, Metasurface-based hybrid optical cavities for chiral sensing, Phys. Rev. Lett. **132**, 043602 (2024).
[13] A. H. Salij, R. H. Goldsmith, and R. Tempelaar, Theory predicts 2d chiral polaritons based on achiral Fabry–Pérot cavities using apparent circular dichroism, Nat. Commun. **15**, 340 (2024).
[14] I. Fernandez-Corbaton, An algebraic approach to light–matter interactions, Adv. Phys. Res. **4**, 2400088 (2025).
[15] D. G. Baranov, C. Schäfer, and M. V. Gorkunov, Toward molecular chiral polaritons, ACS Photon. **10**, 2440 (2023).
[16] G. Fedorovich, D. Kornovan, A. Poddubny, and M. Petrov, Chirality-driven delocalization in disordered waveguide-coupled quantum arrays, Phys. Rev. A **106**, 043723 (2022).
[17] D. G. Suárez-Forero, R. Ni, S. Sarkar, M. J. Mehrabad, E. Mechtel, V. Simonyan, A. Grankin, K. Watanabe, T. Taniguchi, S. Park, H. Jang, M. Hafezi, and Y. Zhou, Chiral flat-band optical cavity with atomically thin mirrors, Sci. Adv. **10**, eadr5904 (2024).
[18] S. Yoo and Q.-H. Park, Metamaterials and chiral sensing: A review of fundamentals and applications, Nanophotonics **8**, 249 (2019).
[19] J. Rosiński, M. Gawełczyk, K. Tarnowski, P. Karwat, D. Wigger, and P. Machnikowski, Quantum dots as optimized chiral emitters for photonic integrated circuits, Phys. Rev. B **109**, 085431 (2024).
[20] V. M. Axt, P. Machnikowski, and T. Kuhn, Reducing decoherence of the confined exciton state in a quantum dot by pulse-sequence control, Phys. Rev. B **71**, 155305 (2005).
[21] R. R. Riso, E. Ronca, and H. Koch, Strong coupling to circularly polarized photons: Toward cavity-induced enantioselectivity, J. Phys. Chem. Lett. **15**, 8838 (2024).
[22] X. Zhong, T. Chervy, L. Zhang, A. Thomas, J. George, C. Genet, J. A. Hutchison, and T. W. Ebbesen, Energy transfer between spatially separated entangled molecules, Angew. Chem. Int. Ed. **56**, 9034 (2017).
[23] D. M. Coles, N. Somaschi, P. Michetti, C. Clark, P. G. Lagoudakis, P. G. Savvidis, and David G. Lidzey, Polariton-mediated energy transfer between organic dyes in a strongly coupled optical microcavity, Nat. Mater. **13**, 712 (2014).
[24] J. Singh, J. Lather, and J. George, Solvent dependence on cooperative vibrational strong coupling and cavity catalysis, ChemPhysChem **24**, e202300016 (2023).
[25] M. V. Imperatore, J. B. Asbury, and N. C. Giebink, Reproducibility of cavity-enhanced chemical reaction rates in the vibrational strong coupling regime, J. Chem. Phys. **154**, 191103 (2021).
[26] J. A. Hutchison, T. Schwartz, C. Genet, E. Devaux, and T. W. Ebbesen, Modifying chemical landscapes by coupling to vacuum fields, Angew. Chem. Int. Ed. **51**, 1592 (2012).
[27] D. F. Kornovan, M. I. Petrov, and I. V. Iorsh, Transport and collective radiance in a basic quantum chiral optical model, Phys. Rev. B **96**, 115162 (2017).
[28] J. S. Peter, S. Ostermann, and S. F. Yelin, Chirality dependent photon transport and helical superradiance, Phys. Rev. Res. **6**, 023200 (2024).
[29] S. De Liberato, Light-matter decoupling in the deep strong coupling regime: The breakdown of the purcell effect, Phys. Rev. Lett. **112**, 016401 (2014).
[30] P. Nataf and C. Ciuti, No-go theorem for superradiant quantum phase transitions in cavity QED and counter-example in circuit QED, Nat. Commun. **1**, 72 (2010).
[31] C. Viviescas and G. Hackenbroich, Field quantization for open optical cavities, Phys. Rev. A **67**, 013805 (2003).
[32] C. Ciuti and I. Carusotto, Input-output theory of cavities in the ultrastrong coupling regime: The case of time-independent cavity parameters, Phys. Rev. A **74**, 033811 (2006).
[33] M. G. Raymer and C. J. McKinstrie, Quantum input-output theory for optical cavities with arbitrary coupling strength: Application to two-photon wave-packet shaping, Phys. Rev. A **88**, 043819 (2013).
[34] L. M. Tomasch, F. Spallek, G. W. Fuchs, T. F. Giesen, and S. Y. Buhmann, Strong coupling of a chiral molecule with circularly polarised modes inside a cavity, arXiv:2412.18700.
[35] Y. Wang and J. Y. Haw, Bridging the gap between the Jaynes–Cummings and Rabi models using an intermediate rotating wave approximation, Phys. Lett. A **379**, 779 (2015).
[36] R. G. Woolley, Power-Zienau-Woolley representations of nonrelativistic QED for atoms and molecules, Phys. Rev. Res. **2**, 013206 (2020).
[37] O. Dmytruk and M. Schiró, Gauge fixing for strongly correlated electrons coupled to quantum light, Phys. Rev. B **103**, 075131 (2021).
[38] G. M. Andolina, F. M. D. Pellegrino, V. Giovannetti, A. H. MacDonald, and M. Polini, Cavity quantum electrodynamics of strongly correlated electron systems: A no-go theorem for photon condensation, Phys. Rev. B **100**, 121109(R) (2019).
[39] O. Viehmann, J. von Delft, and F. Marquardt, Superradiant phase transitions and the standard description of circuit qed, Phys. Rev. Lett. **107**, 113602 (2011).
[40] T. Makihara, K. Hayashida, G. T. Noe, II, X. Li, N. M. Peraca, X. Ma, Z. Jin, W. Ren, G. Ma, I. Katayama, J. Takeda, H. Nojiri, D. Turchinovich, S. Cao, M. Bamba, and J. Kono, Ultrastrong magnon–magnon coupling dominated by antiresonant interactions, Nat. Commun. **12**, 3115 (2021).
[41] S. De Liberato, Comment on "system-environment coupling derived by maxwell's boundary conditions from the weak to the ultrastrong light-matter-coupling regime", Phys. Rev. A **89**, 017801 (2014).
[42] T. M. Autry, G. Nardin, C. L. Smallwood, K. Silverman, D. Bajoni, A. Lemaître, S. Bouchoule, J. Bloch, and S. Cundiff, Excitation ladder of cavity polaritons, Phys. Rev. Lett. **125**, 067403 (2020).
[43] I. Fernandez-Corbaton, M. Fruhnert, and C. Rockstuhl, Objects of maximum electromagnetic chirality, Phys. Rev. X **6**, 031013 (2016).
[44] M. Bamba and T. Ogawa, System-environment coupling derived by Maxwell's boundary conditions from the weak to the ultrastrong light-matter-coupling regime, Phys. Rev. A **88**, 013814 (2013).
[45] D. M. Rouse, E. M. Gauger, and B. W. Lovett, Influence of strong molecular vibrations on decoherence of molecular polaritons, ACS Photon. **11**, 5215 (2024).

[46] gitHub repository, https://github.com/david-dams/chiral-polaritons.

[47] C. Ciuti, G. Bastard, and I. Carusotto, Quantum vacuum properties of the intersubband cavity polariton field, Phys. Rev. B **72**, 115303 (2005).

[48] S. Blanes, F. Casas, J. Oteo, and J. Ros, The magnus expansion and some of its applications, Phys. Rep. **470**, 151 (2009).

[49] M. O. Scully and M. S. Zubairy, Coherent and squeezed states of the radiation field, in *Quantum Optics* (Cambridge University Press, Cambridge, 1997), pp. 46–71.